Geochemistry, Geophysics, Geosystems

RESEARCH ARTICLE
10.1029/2021GC009681

Key Points:

- Numerical models of footwall exhumation show a significant component of solid-block rotation
- Brittle footwall deformation away from the detachment fault is dominated by "apparent unbending"
- "Unbending" since curvature gets reduced, "apparent" as the footwall is not bent in the first place

Supporting Information:

Supporting Information may be found in the online version of this article.

Correspondence to:

D. Sandiford,
dan.sandiford@utas.edu.au

Citation:

Sandiford, D., Brune, S., Glerum, A., Naliboff, J., & Whittaker, J. M. (2021). Kinematics of footwall exhumation at oceanic detachment faults: Solid-block rotation and apparent unbending. *Geochemistry, Geophysics, Geosystems*, *22*, e2021GC009681. https://doi.org/10.1029/2021GC009681

Received 1 FEB 2021
Accepted 23 MAR 2021

Kinematics of Footwall Exhumation at Oceanic Detachment faults: Solid-Block Rotation and Apparent Unbending

Dan Sandiford[1,2], Sascha Brune[2,3], Anne Glerum[2], John Naliboff[4], and Joanne M. Whittaker[1]

[1]Institute for Marine and Antarctic Studies, University of Tasmania, Hobart, TAS, Australia, [2]Helmholtz Centre Potsdam—German Research Centre for Geosciences (GFZ), Potsdam, Germany, [3]Institute of Geosciences, University of Potsdam, Potsdam, Germany, [4]Department of Earth and Environmental Science, New Mexico Institute of Mining and Technology, Socorro, NM, USA

Abstract Seafloor spreading at slow rates can be accommodated on large-offset oceanic detachment faults (ODFs), that exhume lower crustal and mantle rocks in footwall domes termed oceanic core complexes (OCCs). Footwall rocks experience large rotation during exhumation, yet important aspects of the kinematics—particularly the relative roles of solid-block rotation and flexure—are not clearly understood. Using a high-resolution numerical model, we explore the exhumation kinematics in the footwall beneath an emergent ODF/OCC. A key feature of the models is that footwall motion is dominated by solid-block rotation, accommodated by the nonplanar, concave-down fault interface. A consequence is that curvature measured along the ODF is representative of a neutral stress configuration, rather than a "bent" one. Instead, it is in the subsequent process of "apparent unbending" that significant flexural stresses are developed in the model footwall. The brittle strain associated with apparent unbending is produced dominantly in extension, beneath the OCC, consistent with earthquake clustering observed in the Trans-Atlantic Geotraverse at the Mid-Atlantic Ridge.

1. Introduction

Slip accumulation on major normal faults, such as those bounding slow spreading ridges, induces rebound and flexure due to unloading within the axial rift (Buck, 1988; Spencer, 1984; Wernicke & Axen, 1988). The flexural deformation may itself produce brittle failure, representing a cascade of deformation from major to subsidiary fault systems. Slow seafloor spreading is often taken up by extension on large-offset asymmetric detachment faults (ODFs), which exhume lower crustal and mantle rocks in domal footwall exposures termed oceanic core complexes (OCCs) (e.g., Buck, 1993; Cannat, 1993; Lavier et al., 2000; Tucholke, 1998). This study is primarily concerned with the kinematic characteristics of exhumation, the resulting flexural stress and deformation patterns, and the expression of these dynamics in footwall seismicity. We note that throughout the manuscript, we use the terms flexure and bending somewhat interchangeably, in keeping with historical developments in the literature. We use both terms as a description of strain, i.e., relating to changes in curvature. In particular, flexure here does not imply purely elastic constitutive behavior. Indeed, flexural deformations of the lithosphere in our numerical models are dominated by plastic (pseudobrittle) deformation.

Paleomagnetic inclination data show that footwall blocks in ODF systems undergo significant rotation, typically 50–80°, during exhumation; a process that is often termed rollover (Garcés & Gee, 2007; MacLeod et al., 2011; Morris et al., 2009). What remains unclear, however, is whether the kinematics of exhumation (which ultimately produce these estimated rotations) tend to be dominated by footwall flexure (simple bending), solid-block rotation, or perhaps more complicated internal deformation patterns like flexural slip or vertical simple shear (e.g., Wernicke & Axen, 1988). While the kinematics of exhumation has not received a great deal of attention in ODF settings (cf. continental core complexes e.g., Axen & Hartley, 1997; Wernicke & Axen, 1988) a frequent assumption is that flexure plays an important role in footwall exhumation (e.g., Cannat et al., 2019; MacLeod et al., 2002; Parnell-Turner et al., 2017; Schouten et al., 2010; Tucholke, 1998).

This assumption is true not only in regard to the developmental stage of detachments, where regional flexural-isostatic rebound plays a role in rotating planar normal faults to shallower dips, but also in mature settings, with significant (tens km) fault offset. In this view rollover "flexes the brittle footwall, such that the upper part of the footwall block is under tension" (Buck, 1988; Tucholke, 1998). Likewise, the detachment fault itself is thought to "rotate by flexure to low angles" (MacLeod et al., 2002). Again, ridge-parallel faults that intersect OCCs are often depicted as normal faults related to the inferred flexural tension in the upper part of the footwall (Collins et al., 2012; Escartín et al., 2017; MacLeod et al., 2002, 2009; Tucholke et al., 1998). The inferred relationship between OCC/ODF curvature and footwall flexural stress is what we refer to as an "elastic plate model." Such a relationship is completely absent in the numerical models we discuss.

Seismicity provides insight into stress and, particularly, deformation patterns in the brittle lithosphere, and thereby a potential means of constraining kinematics of footwall exhumation. Previous seismicity studies suggest that significant brittle deformation occurs in detachment footwalls as part of exhumation (Demartin et al., 2007; Parnell-Turner et al., 2017). Most records of seismicity in detachment footwalls are dominated by normal-faulting mechanisms and are often attributed to the same far-field tectonic stresses responsible for sustaining the extensional plate boundary (Collins et al., 2012; Demartin et al., 2007; Grevemeyer et al., 2013). Compressional seismicity has also been observed in ODF footwalls, and it is this observation that has been argued to be diagnostic of flexure within the elastic plate framework (Parnell-Turner et al., 2017). However, the identified compressional earthquakes also exhibit significant variability in the orientation of the focal mechanism *P* axes. This casts some doubt over whether such events are representative of a "tectonic" stress state arising from flexure in the detachment system.

In the study of Demartin et al. (2007), which investigated the Trans-Atlantic Geotraverse (TAG) detachment (located on the Mid-Atlantic Ridge at ~26°N), focal mechanisms constructed from footwall seismicity are closely aligned with the spreading direction. The authors identified two distinct zones of seismic activity, one interpreted to represent the curved trace of the active detachment fault, and a second locus approximately 8 km outboard of the detachment cluster, inferred to represent slip on antithetic faults. However, a dynamic explanation for the occurrence of this prominent, spatially offset zone of deformation within the footwall remains elusive.

In this paper, we investigate the kinematics of footwall exhumation beneath an emergent ODF/OCC system, focusing on results from high-resolution numerical models. In these models, solid-block rotation plays a dominant role in the kinematics of footwall exhumation. Our analysis explores the implications for flexural stress and deformation patterns in the system. In doing so, we provide a potential explanation for the seismicity patterns in the TAG detachment, while questioning the tectonic origin for compressional seismicity at the 13°20′N detachment (cf. Parnell-Turner et al., 2017). Our model suggests that flexural strain is an important component of the seismic moment produced in detachment footwalls, however the spatial relationship between flexural strain and detachment curvature is very different to what has commonly been assumed in elastic plate models.

2. Numerical Experiments

We model the evolution of an amagmatic ODF setting using the open source finite element code ASPECT version 2.2.0 (see Bangerth et al., 2020a, 2020b; Heister et al., 2017; Kronbichler et al., 2012). To do so, we solve the incompressible Stokes and advection-diffusion equations, in a 2-D domain, subject to boundary conditions on the temperature and velocity. The model is initialized with a thin lithosphere, defined by a transient cooling profile with a thermal age of 0.5 Myr in the center of the domain. The domain is 400 km wide and 100 km deep. The thermal profile ages outwardly in proportion to the applied spreading rate of 2 cm/yr (full rate), which is representative for slow ocean ridges in general and similar to the current spreading rate at the TAG detachment (~2.5 cm/yr) (Müller et al., 2016). Uniform inflow at the bottom boundary balances the outward flux of material at the side boundaries. The model has a free surface (Rose et al., 2017), and a diffusion process is applied to the surface topography in order to counteract strong mesh deformation. A simplification here is that the effect of the water column is ignored, i.e., the detachment is modeled as subaerial. The model has a static, hierarchical mesh refinement, where the square elements

can be locally refined by division into four smaller squares. In this study we focus on the brittle part of the model, where we successively refine the elements until they feature an edge length of 125 m, while in the deeper parts of the model the element length is 2 km.

There is no compositional differentiation in the model (i.e., no crust/mantle). All parts of the domain are subject to the same constitutive model. The constitutive model incorporates viscous (dislocation creep), elastic, and plastic (pseudobrittle) deformation mechanisms, hereafter referred to as viscoelastic plastic (VEP) rheology, following the approach of Moresi et al. (2003). The development and benchmarking of the rheological model was guided by the study of Olive et al. (2016). The dominant deformation mechanism is selected for each element based on the system state (temperature, stress, accumulated strain). A random component of plastic strain is used to localize deformation. Further details and employed parameters are provided in supporting information S2, and Table S1. The ASPECT parameter file used to run the reference model can be downloaded from https://github.com/dansand/odf_paper, or from the supporting information.

The development of detachment fault systems is associated with the existence of faults that are significantly weaker than the host rock (Buck, 1993; Forsyth, 1992; Reston & Ranero, 2011), while the additional development of rider blocks can depend on the relative amount of weakening in the cohesion versus friction coefficient terms in the yield stress envelope (Choi et al., 2013). Here, we applied strain weakening of cohesion, friction angle and the viscosity associated with dislocation creep, similar to recent studies using ASPECT (Glerum et al., 2018; Naliboff et al., 2020). These parameters are provided in the supporting information.

The reference model (e.g., Figure 1) develops a large-offset OCC (several tens km), in the absence of rider blocks (see Figure 3 annotations for clarification) and remains in a quasi steady state for around 1 Myr, until the footwall breaks up and a new detachment emerges. These timescales are consistent with the observed duration of individual OCCs segments (Tucholke et al., 1998). In addition, we present an alternative model (e.g., Figure 3) where the rate of plastic weakening is faster (cohesion/friction angle reduce linearly by factors of 0.5/0.1 over a strain interval of 2, rather than 6). In this model, the footwall shows a greater tendency to break up, similar to previous modeling results (Lavier et al., 2000).

3. Model Evolution, Kinematics, and Deformation

3.1. Reference Model Evolution

Figure 1 shows the evolution of the reference model from a brief stage of symmetrical necking through to a completely asymmetric ODF system. At 0.1 Myr (2 km total extension), near-symmetric planar faults are active, producing a graben with minor intrarift faults. The load (deficit) of the graben is supported through regional flexural-isostatic rebound, as revealed in the horizontal component of the deviatoric stress tensor in the left-hand panels of Figure 1. This is one of two modes of lithospheric flexure exhibited by the model, as discussed later.

At 0.3 Myr (6 km total extension) the flexural-isostatic response has deformed the active faults, with an overall rotation to lower dip, and with the deeper parts of each conjugate fault adopting a curved, concave-down shape (cf. Buck, 1988; Olive & Behn, 2014). At around this point, the model rapidly transitions to asymmetric extension. The left-dipping fault begins to sole into a wider zone of ductile shear at the brittle-ductile transition (see also Figure 2a). Meanwhile the conjugate fault is abandoned. At this point, the flow of mantle material into the footwall of the active fault develops a strong solid-block rotation component (as highlighted by the vorticity field, right-hand panels Figure 1).

Beyond 0.3 Myr (>6 km total extension), slip along the detachment fault leads to the progressive up-dip migration of the breakaway zone, and exposure of the OCC (refer to annotations in Figure 2 as a guide to terminology). Between ~1.0 and 2.0 Myr (20–40 km total extension), the geometry and kinematics of the system reach quasi steady state. After about 2.4 Myr (~50 km total extension), the footwall begins to break up, with an antithetic footwall fault becoming the locus for a new, oppositely dipping, detachment. This stage of the model development is shown in the Movie S1.

The most important insight we draw from our numerical models is the way in which detachment fault concavity is closely tied to the development of solid-block rotation in the footwall (e.g., Figure 1 right-hand

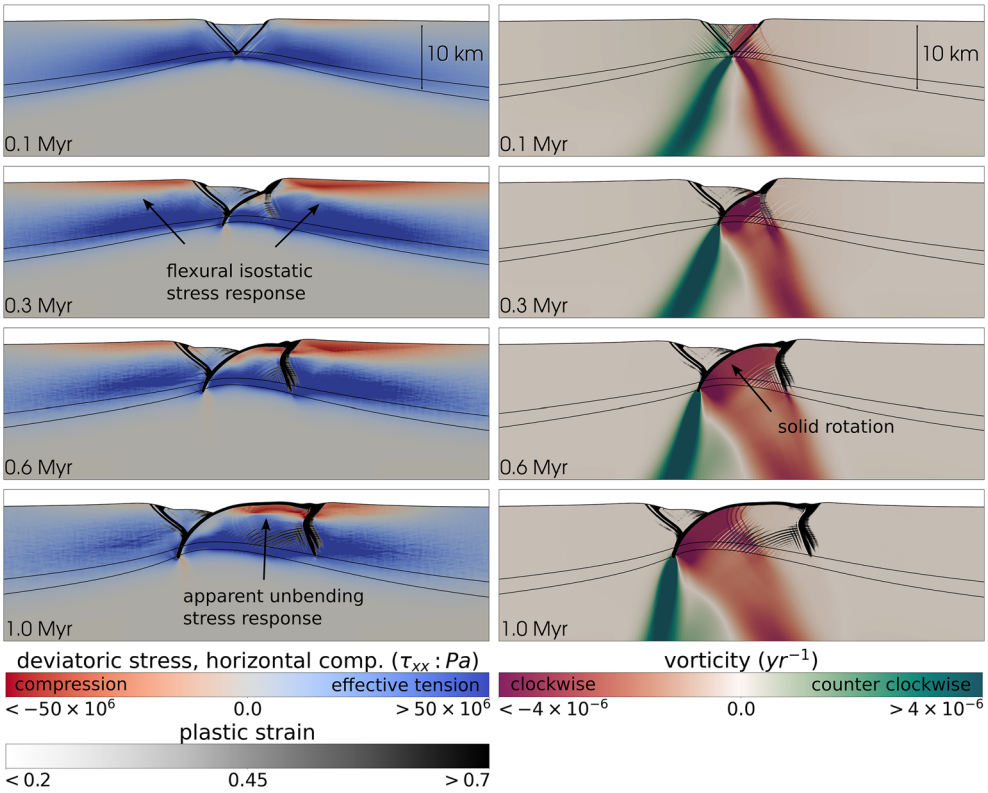

Figure 1. Evolution of reference numerical model from symmetric graben to asymmetric detachment system highlighting the role of solid-block rotation in exhumation as well as flexural processes. The left-hand panels show horizontal component (τ_{xx}) of the deviatoric stress tensor, revealing flexural stress accumulation during the development of the ODF and footwall exhumation. The stress tensor definition, for the Maxwell viscoelastic plastic rheology, is discussed in the supporting information. The right-hand panels show the vorticity (counter-clockwise rotations are positive), and highlight the role of solid-block rotation. The two black lines are contours of the temperature field at 600 and 700°C. The accumulated plastic strain is shown with a transparent greyscale, showing the location of brittle structures. The full model evolution is animated in Movie S1. The aspect ratio of this figure is 1. ODF, oceanic detachment fault.

panels). This aspect of the exhumation kinematics has significant impact on how flexure operates in the system, which we elaborate in the rest of the manuscript.

3.2. Exhumation Kinematics

Figure 2 shows features of the reference model after 1.5 Myr of evolution, when the detachment system has reached a quasi-steady state (in the hanging wall reference frame). In Figure 2a, we show the square root of second invariant (hereafter magnitude) of the strain rate tensor as well as the model velocity vectors. In Figure 2b, we show the flow vorticity as well as vectors of the translated velocity field (velocity in the hanging wall reference frame).

In the footwall directly beneath the ODF, the combination of relatively high vorticity and low strain rate magnitude indicates flow dominated by solid-block rotation. This rotation is accommodated by the morphology of the active ODF, which approximates a circular arc through much of its active extent. Note that the zone of high vorticity in the footwall extends slightly deeper than the base of the brittle-ductile transition (~700°C as shown by the limit of plastic strain development in Figure 2d). As we explain in the Discussion, this provides the explanation for why the footwall does not exhibit the stress state anticipated in the elastic stress model (i.e., tension in the upper-most part of the footwall, with compression at greater depths).

With solid-block rotation dominant in the footwall beneath the ODF, and rigid plate motion occurring in the outboard region (i.e., toward the right-hand side of the model), it follows that there must be a transitional

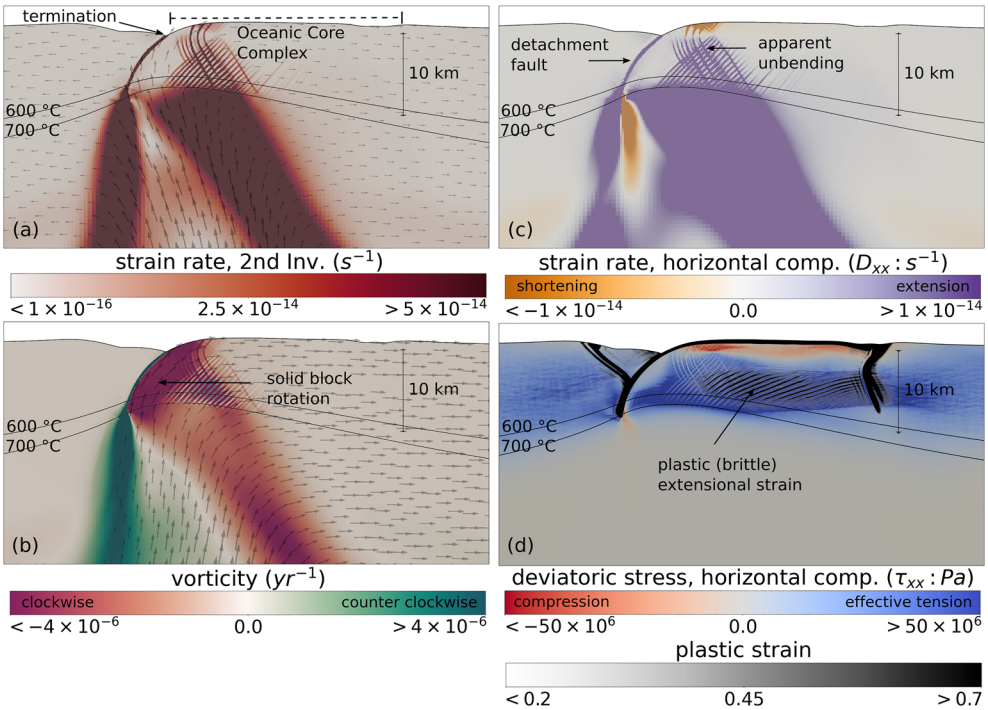

Figure 2. Reference model at an elapsed time of 1.5 Myr, in a quasi-steady state configuration, showing strain localization in the footwall outboard from the termination (apparent unbending), and solid-block rotation in the footwall beneath the ODF. Annotations show key features of the detachment system referred to in main text. (a) Square root of the second invariant of the strain rate. Model velocity is shown with arrows. Black lines are temperature contours at 600 and 700°C, within which the brittle-ductile transition occurs. (b) Flow vorticity. Arrows show the velocity in the hanging wall reference frame (in which the system is quasi steady state). (c) Horizontal component (D_{xx}) of the strain rate tensor. (d) Horizontal component of the deviatoric stress tensor (τ_{xx}) overlaid with the accumulated plastic (pseudobrittle) strain. The aspect ratio of this figure is 1. ODF, oceanic detachment fault.

zone between these flow regimes. In the reference model, this transition occurs as a zone of flexural deformation outboard from the active ODF, beneath the OCC. The flexural nature of the deformation is revealed by the polarized pattern in the horizontal deformation rate (Figure 2c) with shortening in the upper few kilometers and a significantly larger, triangular zone of active extension in the deeper part of the footwall.

We refer to this zone of flexural deformation as the zone of "apparent unbending." "Unbending" because the flexural strain (change in curvature) is essentially measurable by the straightening of the ODF, "apparent" because the ODF footwall in our model is not really bent in the first place. In other words, apparent unbending is a stress-accumulating rather than a stress-releasing process (in contrast to the elastic plate model). The spatial relationship between the zone of apparent unbending and ODF curvature is covered in more detail in Section 4.

3.3. Effects of Rapid Strain Weakening

Figure 3 shows strain rates and vorticity from an alternative model where the rate of plastic weakening is faster (cohesion/friction angle reduce by factors of 0.5/0.1 over a strain interval of 2, rather than 6). This inhibits the development of large displacement, quasi steady state detachment systems. Instead, we see more rapid reorganizations, along with various modes of "rider block" formation and footwall breakup. The model evolution is shown in more detail in Movie S2. Although the alternative model displays greater structural complexity and temporal variability than the reference model, exhumation of the footwall is likewise associated with a strong component of solid-block rotation, shown by high (negative) values in the right-hand panels of Figure 3.

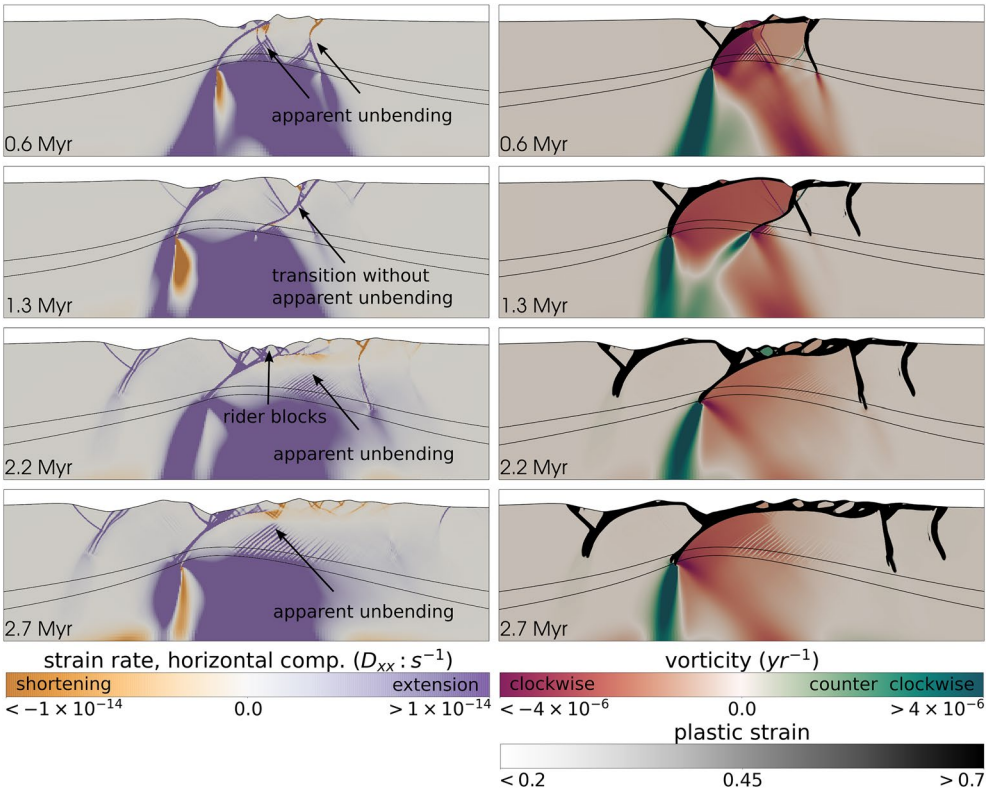

Figure 3. Evolution of the alternative model with more rapid strain weakening, highlighting the role of solid-block rotation in the footwall beneath the ODF. Footwall deformation shows greater structural complexity that the reference model, including rider block formation. The left-hand panels show the horizontal component (D_{xx}) of the strain rate tensor. The right-hand panels show the vorticity, along with the accumulated plastic strain in semitransparent greyscale. The two black lines are contours of the temperature field at 600 and 700°C. The model evolution is shown in more detail in Movie S2. The aspect ratio of this figure is 1. ODF, oceanic detachment fault.

In the previous section, we discussed the kinematic requirement that deformation must take place between the exhumation region, where the footwall is dominated by solid-block rotation, and the outboard region where the plate undergoes rigid translation. In the reference model, this transition occurs through a process of brittle flexure (apparent unbending). The alternative model also undergoes periods when the transition occurs through apparent unbending (e.g., snapshots at 0.6, 2.2, and 2.7 Myr). However, the alternative model demonstrates that the kinematic transition can instead occur through slip on a single through-going normal fault. This pattern is shown in the snapshot at 1.3 Myr.

At this point, the footwall does not "apparently unbend" in a coherent (flexural) manner, but rather it undergoes rotation as an almost-rigid block, bounded by major faults at either end (one being the ODF). The fault at the outboard edge on the right-hand side of the block has a concave-up geometry, as is required to accommodate the rotation, in a sense mirroring that of the ODF, and it becomes sub-vertical near its surface exposure. This mode of footwall transition has some similarities with the 'subvertical simple shear' model, arising from an analogous kinematic problem in the context of continental core complexes (Wernicke & Axen, 1988), while a similar mode of footwall faulting was observed in numerical simulations of Bickert et al. (2020).

Two aspects of the system are notable at this stage (i.e., 1.3 Myr in Figure 3). First, the kinematic transition between rotation and translation is achieved without any shallow footwall shortening (unlike in the case of apparent unbending). Second, the footwall exposure (OCC) at this stage has a domal shape, where material is rotationally overturned, such that the slope and velocity vector at the outboard edge of the OCC have a downwards component (velocity vectors are shown in Movie S2).

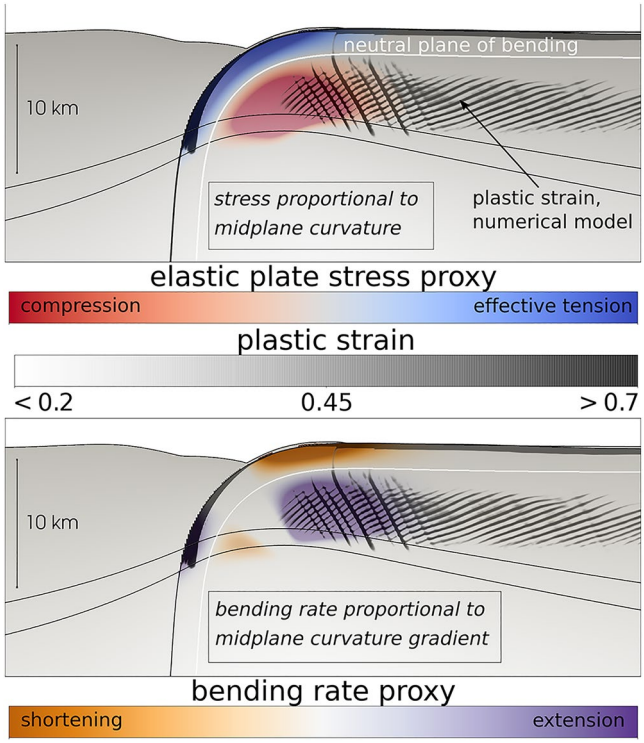

Figure 4. Schematic showing proposed relationships between the detachment geometry and the footwall dynamics (e.g., stress and strain rate). Colored fields are illustrative, and are not derived from a numerical model. The top panel represents an elastic plate relationship for footwall stress, where flexural stress (red-blue) is proportional to the curvature of the ODF/OCC (a relationship that is absent in our numerical models). The bottom panel illustrates a process that is much more relevant to our numerical model, where (advective) bending rates (shown in gold-purple) are proportional to the curvature gradient of the ODF/OCC. This results in a zone of flexural strain in the footwall outboard of the termination (apparent unbending). Further information about the generation of these colored ("proxy") fields is provided in the supporting information. In both panels the accumulated plastic strain from our reference numerical model is shown (at an elapsed time of 2.0 Myr) in greyscale. This highlights how the plastic strain in the footwall (faults) is mainly produced in the lower (extensional) part of the zone of apparent unbending (purple region bottom panel). The aspect ratio of this figure is 1. ODF, oceanic detachment fault; OCC, oceanic core complex.

4. Discussion

There are two main focus points of our discussion. First, we consider flexural processes in our numerical models in more detail, highlighting contrasts with existing models for the flexural stress in ODF systems. Second, we compare the modeled patterns of brittle deformation with observations of seismicity.

4.1. Flexural Processes in Footwall Exhumation

Strain rates and stresses in our numerical models suggest an important role for flexure in footwall exhumation. The main locus of flexure in the reference model (e.g., Figure 2) occurs outboard from the ODF termination, associated with shortening in the upper few kilometers of the OCC/footwall and extension beneath the neutral plane. We describe this process as apparent unbending.

This flexural pattern is very different from that expected based on an elastic plate model, which has commonly been invoked for the flexural stress state of the footwall. In this view, rollover actively "*flexes the brittle footwall, such that the upper part of the footwall block is under tension*" (Tucholke, 1998). Recently, the discovery of compressional earthquake focal mechanisms in an ODF footwall has been interpreted in terms of an elastic-plastic plate model, which shares a subtle but important assumption (with the elastic plate model) that the geometry of the ODF/footwall records a history of monotonic curvature increase (Parnell-Turner et al., 2017). To understand the flexure patterns produced in our numerical models, and why these diverge from the expectation of an elastic (or elastic-plastic) plate model, we need to carefully consider both the mechanical and kinematic trajectory of the upwelling rock mass during exhumation.

Deviatoric stresses in the models (e.g., Figures 1 and 2d) decrease dramatically at temperatures above the 700°C isotherm, which corresponds closely with the brittle-ductile transition (BDT). Importantly, as upwelling footwall material crosses the BDT, the flow field is already dominated by a solid-block rotational component (Figure 2b). Hence, there is no process of curvature increase (at least within the brittle-elastic regime) to produce the stress state envisaged in an elastic plate model. How deformation is resolved beneath the BDT (in order for this rotational flow to develop) is of little consequence, as the deviatoric stresses produced are negligible (due to the efficacy of viscous relaxation). In simple terms: rotation develops before strength. It is for this reason that the ODF curvature is representative of a neutral stress configuration, rather than a bent one.

In the previous section, we discussed the kinematic requirement that deformation must take place between the exhumation region where the footwall is dominated by solid-block rotation, and the outboard region where the plate undergoes rigid translation. In the reference model, this process occurs through a zone of inelastic (plastic/brittle) flexure, i.e., apparent unbending (Figure 2c). The footwall follows the trend of decreasing curvature in bathymetry outboard of the detachment termination. We can also view apparent unbending as being a result of a finite advective curvature rate, which is proportional to curvature gradients (e.g., Figure 4) (Kawakatsu, 1986; Sandiford et al., 2020). As a result, counter-intuitively, material in the footwall undergoes virtually monotonic flexural strain with exactly the opposite polarity to that implied by the detachment curvature.

This notion of the advective curvature rate emphasizes an important aspect of apparent unbending, which is that significant flexural deformation rates can be present even when the morphology of the system is static. This view also helps differentiate the mode of apparent unbending from ordinary flexural-isostastic adjustment, wherein flexural deformation is only present in the case of changing loads. To aid these discussion points, the contrasts between an elastic plate model of stress and the flexural bending rates that are associated with apparent unbending are illustrated in Figure 4.

In the zone of apparent unbending, deformation tends to localize strongly, for instance producing the ≤10 km wide zone of flexure in the footwall of the reference model (e.g., Figure 2c). In contrast, the resulting flexural stress patterns are present over much broader region. Indeed, the stress response to apparent unbending is, to a significant degree, imprinted in the plate as it moves off-axis (e.g., Figure 2d). This is an important observation for thinking about how to interpret patterns of seismicity from a geodynamic perspective; i.e., should variations in seismic moment (or activity rate) be compared with patterns of differential stress or rather strain rates (or a combination of both, e.g., the brittle dissipation)? Our interpretative framework is motivated by Chapple and Forsyth (1979) who argue that seismicity should be viewed as the expression of strain in the brittle regime. In this view, zones of high brittle strain rate, along with the orientation of deformation, are the most relevant quantities to compare to earthquake observations.

While the alternative numerical model (Figure 3) shows a more complex evolution, exhumation is likewise dominated by solid-block rotation. Hence, the same general conclusions follow in regard to the fact that detachment curvature is a misleading proxy for flexural stress.

To our knowledge, the process of apparent unbending has not been discussed in previous modeling studies nor its relationship to solid-block rotation in detachment footwalls. Yet a number of previous numerical models show strain rate patterns consistent with this kinematic feature. Figures 2b and 2c of the 2-D models of Tucholke et al. (2008) show a zone of high strain rate outboard of the surface ODF exposure. The geometry of this zone shows a characteristic triangular hourglass pattern, suggestive of flexural strain. A similar feature can be discerned in the 3-D models of Howell et al. (2019), although the vertical exaggeration makes the pattern less clear. In both cases, only the magnitude of the stain rate tensor is shown (rather than its horizontal components), so the flexural nature of the deformation cannot be identified with complete confidence. Nevertheless, it appears that the kinematic processes we have identified in our model are evident in previous numerical modeling studies.

4.2. Flexure and Brittle Deformation in Models

The accumulated plastic (pseudobrittle) strain in the reference model is shown in Figure 2d (at 1.5 Myr) and Figure 4 (at 2.0 Myr). Comparing the zone of plastic strain accumulation with the sign of the stress or strain rate horizontal components (e.g., Figure 2c) reveals that the plastic strain accumulated during exhumation is almost entirely generated by extensional structures in the region of apparent unbending. These patterns in the accumulated plastic strain show that while there is a flexural origin for most of the brittle strain in the detachment footwall, its seismic expression is expected to be dominated by normal faulting.

Earlier in the reference model development, footwall faulting is characterized by normal faults synthetic to the ODF (e.g., Figure 2 at 1.5 Myr). Later in the model, we see a systematic spatial trend where extension occurs on closely spaced ODF-synthetic normal faults nearer the axial valley, moving outboard to more widely spaced antithetic faults. Note how in Figure 4, these larger antithetic faults can be seen to offset the synthetic-dipping faults. Ultimately, one of the major antithetic normal faults becomes the structure on which a new detachment fault forms, reversing the dip of the detachment (as is shown in Movie S1).

4.3. Observational Constraints and Predictions

In the previous sections, we summarized kinematic and deformation patterns in our numerical models. We now discuss these patterns in connection to observations of seismicity from ODF/OCC segments. Recording small magnitude events and obtaining precise earthquake hypocenters in ODF regions generally requires hydrophone or ocean-bottom seismograph deployment. Hence, at this stage only a small number of pertinent studies exist (Collins et al., 2012; Demartin et al., 2007; Grevemeyer et al., 2013; Parnell-Turner

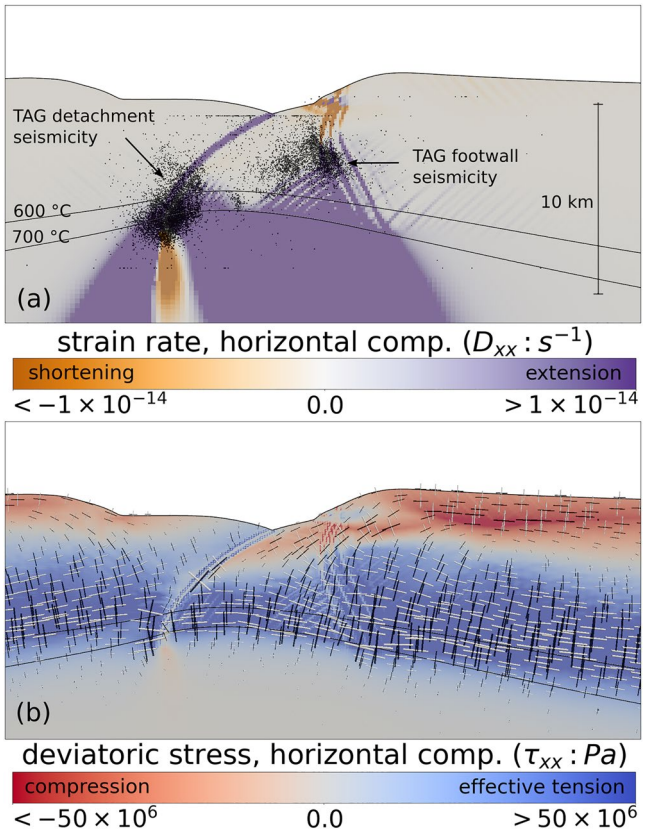

Figure 5. Comparison of model detachment/exhumation dynamics with seismicity from the TAG segment, which has a similar horizontal offset of (~5 km) between the detachment termination and breakaway. Both panels show features of the reference model at an elapsed time of 0.4 Myr, after 8 km total extension. (a) Horizontal component (D_{xx}) of the strain rate tensor. In the footwall, strain is localized strongly in the zone of apparent unbending. Black dots show seismicity from a swathe of hypocenters from the TAG segment, mainly representing normal fault mechanisms (from Demartin et al. (2007)). The relative location of these events is established based on the detachment location and with reference to the original study. (b) Horizontal component of the deviatoric stress (τ_{xx}). Flexural stress in the footwall is much less localized than strain rates (i.e., panel (a)). Black vectors show the orientation and relative magnitude of most compressive principal stress τ_1, white vectors show most extensive principal stress τ_3. The aspect ratio of this figure is 1. TAG, Trans-Atlantic Geotraverse.

et al., 2017, 2020; Yu et al., 2018). Even fewer show a pattern of hypocenters in which a dominant asymmetric detachment is convincingly delineated, which would suggest a tectonic configuration analogous to our model setup.

Figure S1 shows map and cross-sectional views of the hypocenters at the TAG detachment from Demartin et al. (2007). In Figure 5, we plot a narrow swathe (those epicenters ≤ 4.5 km of the line shown in Figure S1) of the TAG earthquakes overlaid on the horizontal strain rate component from our model. This exercise suggests that important features of the TAG detachment seismicity can be explained by the kinematic and flexural patterns we have discussed. In particular, the combination of solid-block rotation beneath the detachment and apparent unbending beneath the OCC may explain why the TAG footwall directly beneath the ODF has sparse seismicity, while extensional seismicity is concentrated outboard of the termination. It can also explain why footwall seismicity is concentrated at depths greater than ~2 km beneath the seafloor (see Figure S1 for location of seismicity relative to the TAG bathymetry).

Nevertheless, it is clear the footwall earthquake cluster imaged by Demartin et al. (2007) is significantly more limited in its spatial extent than compared to the region of high strain rates developed in the model (e.g., Figure 5). A few points are worth bearing in mind, however: the seismic deployment detailed in Demartin et al. (2007) was relatively short (8 months), and seismicity patterns may be biased with respect to the long-term tectonic strain rates; there may be additional variability in terms of whether faulting occurs as unstable sliding versus aseismic slip (Mark et al., 2018), as well as the level of microseismicity versus larger events (i.e., the *b* value). Similarly, procedures on the numerical modeling side could be implicated: we omit physical processes such as melting, hydrothermal heat transport as well as any three-dimensional aspects of dynamics which may affect thermal and dynamic structure of the footwall. Moreover, the constitutive models utilized in our simulations, convergence of associated nonlinearity, and the implications of mesh sensitivity, are areas of active research, debate and experimentation for the geodynamic discipline (e.g., Duretz et al., 2020). It will therefore be important to explore whether the kinematic features we identify are equally prominent in the models of other groups that use different numerical approaches, constitutive models and physical approximations.

Our numerical models do not offer a ready explanation for compressional seismicity directly beneath the ODF, as reported by Parnell-Turner et al. (2017). However, these compressional earthquakes also exhibit significant variability in the orientation of the focal mechanism *P* axes (unlike the cluster attributed to the detachment fault itself—Figure 2c of that study). This is a potential indication that these earthquakes do not have a tectonic origin, or at least that the causes for deformation cannot be reduced to 2-D plane-strain processes like elastic plate bending or apparent unbending. We note that in a follow-up study of this region, which also encompasses areas directly to the north, the vivid cluster of compressional events is absent (Parnell-Turner et al., 2020). Rather, this later study mainly captures earthquakes inferred to belong to the detachment faults, as well as streaks of activity outboard of the axial valley beneath the OCC/footwall. In the 13°30′N detachment region, for instance, clustering is broadly comparable to the TAG patterns, although event numbers are smaller.

A prediction of our reference numerical model is that a small amount of shortening may occur in the shallowest few kilometers of OCCs, associated with the process of apparent unbending. The steep thrust structures that accommodate this strain have a total downdip extent of only a few kilometers, and they are

expected to contribute a very minor part of the total seismic moment associated with footwall exhumation (see the patterns of accumulated plastic strain in Figure 4). While such deformation may be difficult to capture in the short-term seismic record, these steeply dipping reverse faults represent the active structures that should intersect exposed OCCs, in places where they tend to flatten (curvature reduction) outboard of the detachment termination.

OCCs are known to be dissected by spreading-perpendicular faults, although there is clearly much variability, such as observed at the adjacent Mid-Atlantic Ridge detachments at ~13°20′N (no obvious dissecting faults) and 13°30′N (with dissecting faults), e.g., Parnell-Turner et al. (2018). In the case of 13°30′N detachment, such dissecting faults have been interpreted as reflecting the along-axis propagation of a magmatic source into the abandoned detachment system (Escartín et al., 2017). In other instances, dissecting faults are attributed to extensional bending stresses during footwall rollover (Escartín et al., 2003; Tucholke et al., 1998), i.e., invoking an elastic plate stress relationship. In the Suckling-Dayman continental core complex in Papua New Guinea, steep contractional faults have been identified that post-date exhumation (Little et al., 2019). Biemiller et al. (2019) have previously linked this observation to the prediction of near-surface shortening in a numerical model of detachment faulting.

The alternative numerical model shows that footwall rotation during exhumation is not always associated with apparent unbending (i.e., Figure 3 snapshot at 1.3 Myr). The transition from rotation to rigid plate translation can instead occur via a major through-going fault at the outboard edge of the block. Hence, our model results should not be interpreted as suggesting that all OCC footwalls must undergo apparent unbending and hence exhibit evidence of minor thrust faults. Rather, the key prediction of the models is that exhumation beneath concave-down ODFs is dominated by solid-block rotation. The zone of solid-block rotation must transition, via some pattern of deformation, to the outboard region of rigid plate translation. Our models show two modes in which this may occur. We suggest that where exposed OCCs reduce their curvature outboard of the ODF termination, yet remain largely coherent, the flexure should be associated with shortening, compressional stress accumulation, and minor, probably steeply dipping, thrust faults.

5. Conclusions

This study addresses the nature of footwall exhumation in ODF settings, based on results of high-resolution numerical models. Exhumation is characterized by a strong component of solid-block rotation, accommodated by the concave-down ODF. This has important implications for how flexural processes operate in the system. We demonstrate a relationship between flexural stress and detachment curvature that is very different to the elastic plate model commonly assumed. Our model also helps differentiate between the static flexural stress component associated with regional compensation of the axial depression, and a kinematic component of flexure associated with the transition from solid-block rotation of the footwall to rigid plate translation (apparent unbending).

Our results suggest that flexure related to apparent unbending may provide a significant component of the extensional seismic moment in detachment footwalls. Whereas Parnell-Turner et al. (2017) argued that bending may cause "compression in extension," our models rather suggests that bending may promote "extension in extension." The deformation patterns predicted in our model are broadly applicable to microseismicity patterns from the TAG detachment.

Classical models of detachment systems propose that normal faults originate at high angle and continuously rotate flexurally to a low-angle (Buck, 1988; Wernicke & Axen, 1988). Accordingly, footwall exhumation is often assumed to involve active flexure in the sense defined by the detachment curvature (Tucholke et al., 1998). In the numerical models discussed here, rotation of the footwall during exhumation is instead dominated by solid-block rotation, accommodated by the concave-down detachment geometry. In this way, the mature detachment fault appears to be acting less as a classical fault and more in the sense of an exhumation channel (Brune et al., 2014). Instead of representing progressive flexural rotation of the fault to a nonoptimal dip, the concave-down curvature is simply the geometric configuration that facilitates solid rotation of the footwall. We speculate that minimization of distributed plastic strain may play a role in this configuration.

Nevertheless, flexural isostasy does seem to play a role in producing the initial transition from steep planar fault into a concave-down geometry (as in Buck (1988)). To paraphrase Olive and Behn (2014), faults experience advection in the displacement field induced by the footwall flexure. Hence there seems to be a subtle transition from initial deformation of the fault, tied to flexural isostasy, to a stage in which the fault curvature seems increasingly dynamically linked to solid rotation in the footwall. Such details provide an avenue for future research into these enigmatic plate boundary zones.

Data Availability Statement

Data are available through Demartin et al. (2007) (10.1594/IEDA/306798).

Acknowledgments
Figures were created using Pyvista, a Python interface for the Visualization Toolkit (VTK) (Sullivan & Kaszynski, 2019). Dan Sandiford, Sascha Brune, and Joanne M. Whittaker were supported by Australian Research Council Grant DP180102280. Anne Glerum was supported by the Helmholtz Young Investigators Group CRYSTALS (Grant No. VH-NG-1132). We thank Jean-Arthur Olive and Garrett Ito for their constructive reviews of the paper. The work was supported by the North-German Supercomputing Alliance (HLRN). Dan would like to acknowledge Mike Sandiford for his enthusiasm and support; congratulations on a wonderful innings Mike!

References

Axen, G. J., & Hartley, J. M. (1997). Field tests of rolling hinges: Existence, mechanical types, and implications for extensional tectonics. *Journal of Geophysical Research*, *102*(B9), 20515–20537. https://doi.org/10.1029/97JB01355

Bangerth, W., Dannberg, J., Gassmoeller, R., & Heister, T. (2020a). *Aspect v2.2.0*. Zenodo. https://doi.org/10.5281/zenodo.3924604

Bangerth, W., Dannberg, J., Gassmöller, R., Heister, T. (2020b). *Aspect: Advanced solver for problems in Earth's ConvecTion, user manual*. https://doi.org/10.6084/m9.figshare.4865333

Bickert, M., Lavier, L., & Cannat, M. (2020). How do detachment faults form at ultraslow mid-ocean ridges in a thick axial lithosphere? *Earth and Planetary Science Letters*, *533*, 116048. https://doi.org/10.1016/j.epsl.2019.116048

Biemiller, J., Ellis, S., Mizera, M., Little, T., Wallace, L., & Lavier, L. (2019). Tectonic inheritance following failed continental subduction: A model for core complex formation in cold, strong lithosphere. *Tectonics*, *38*, 1742–1763. https://doi.org/10.1029/2018TC005383

Brune, S., Heine, C., Pérez-Gussinyé, M., & Sobolev, S. V. (2014). Rift migration explains continental margin asymmetry and crustal hyper-extension. *Nature Communications*, *5*(1), 1–9. https://doi.org/10.1038/ncomms5014

Buck, W. R. (1988). Flexural rotation of normal faults. *Tectonics*, *7*(5), 959–973. https://doi.org/10.1029/tc007i005p00959

Buck, W. R. (1993). Effect of lithospheric thickness on the formation of high- and low-angle normal faults. *Geology*, *21*(10), 933–936. https://doi.org/10.1130/0091-7613(1993)021<0933:EOLTOT>2.3.CO;2

Cannat, M. (1993). Emplacement of mantle rocks in the seafloor at mid-ocean ridges. *Journal of Geophysical Research*, *98*(B3), 4163–4172. https://doi.org/10.1029/92JB02221

Cannat, M., Sauter, D., Lavier, L., Bickert, M., Momoh, E., & Leroy, S. (2019). On spreading modes and magma supply at slow and ultraslow mid-ocean ridges. *Earth and Planetary Science Letters*, *519*, 223–233. https://doi.org/10.1016/j.epsl.2019.05.012

Chapple, W. M., & Forsyth, D. W. (1979). Earthquakes and bending of plates at trenches. *Journal of Geophysical Research*, *84*(B12), 6729–6749. https://doi.org/10.1029/jb084ib12p06729

Choi, E., Buck, W. R., Lavier, L. L., & Petersen, K. D. (2013). Using core complex geometry to constrain fault strength. *Geophysical Research Letters*, *40*, 3863–3867. https://doi.org/10.1002/grl.50732

Collins, J. A., Smith, D. K., & McGuire, J. J. (2012). Seismicity of the Atlantis massif detachment fault, 30 n at the mid-Atlantic ridge. *Geochemistry, Geophysics, Geosystems*, *13*, Q0AG11. https://doi.org/10.1029/2012GC004210

Demartin, B. J., Sohn, R. A., Pablo Canales, J., & Humphris, S. E. (2007). Kinematics and geometry of active detachment faulting beneath the trans-atlantic geotraverse (tag) hydrothermal field on the mid-Atlantic ridge. *Geology*, *35*(8), 711–714. https://doi.org/10.1130/g23718a.1

Duretz, T., de Borst, R., Yamato, P., & Le Pourhiet, L. (2020). Toward robust and predictive geodynamic modeling: The way forward in frictional plasticity. *Geophysical Research Letters*, *47*, e2019GL086027. https://doi.org/10.1029/2019GL086027

Escartín, J., Mével, C., MacLeod, C. J., & McCaig, A. (2003). Constraints on deformation conditions and the origin of oceanic detachments: The mid-atlantic ridge core complex at 15°45′N. *Geochemistry, Geophysics, Geosystems*, *4*(8), 1067. https://doi.org/10.1029/2002GC000472

Escartín, J., Mével, C., Petersen, S., Bonnemains, D., Cannat, M., Andreani, M., et al. (2017). Tectonic structure, evolution, and the nature of oceanic core complexes and their detachment fault zones (13°20′N and 13°30′N, Mid Atlantic Ridge) Tectonic structure, evolution, and the nature of oceanic core complexes and their detachment fault zones (13°20′N and 13°30′N, mid Atlantic ridge). *Geochemistry, Geophysics, Geosystems*, *18*, 1451–1482. https://doi.org/10.1002/2016GC006775

Forsyth, D. W. (1992). Finite extension and low-angle normal faulting. *Geology*, *20*(1), 27–30. https://doi.org/10.1130/0091-7613(1992)020<0027:FEALAN>2.3.CO;2

Garcés, M., & Gee, J. S. (2007). Paleomagnetic evidence of large footwall rotations associated with low-angle faults at the mid-Atlantic ridge. *Geology*, *35*(3), 279–282. https://doi.org/10.1130/g23165a.1

Glerum, A., Thieulot, C., Fraters, M., Blom, C., & Spakman, W. (2018). Nonlinear viscoplasticity in aspect: Benchmarking and applications to subduction. *Solid Earth*, *9*, 267–294. https://doi.org/10.5194/se-9-267-2018

Grevemeyer, I., Reston, T. J., & Moeller, S. (2013). Microseismicity of the Mid-Atlantic Ridge at 7°S-8°15′S and at the Logatchev Massif oceanic core complex at 14°40′N-14°50′N. *Geochemistry, Geophysics, Geosystems*, *14*, 3532–3554. https://doi.org/10.1002/ggge.20197

Heister, T., Dannberg, J., Gassmöller, R., & Bangerth, W. (2017). High accuracy mantle convection simulation through modern numerical methods—II: Realistic models and problems. *Geophysical Journal International*, *210*(2), 833–851. https://doi.org/10.1093/gji/ggx195

Howell, S. M., Olive, J.-A., Ito, G., Behn, M. D., Escartín, J., & Kaus, B. (2019). Seafloor expression of oceanic detachment faulting reflects gradients in mid-ocean ridge magma supply. *Earth and Planetary Science Letters*, *516*, 176–189. https://doi.org/10.1016/j.epsl.2019.04.001

Kawakatsu, H. (1986). Double seismic zones: Kinematics. *Journal of Geophysical Research*, *91*(B5), 4811–4825. https://doi.org/10.1029/jb091ib05p04811

Kronbichler, M., Heister, T., & Bangerth, W. (2012). High accuracy mantle convection simulation through modern numerical methods. *Geophysical Journal International*, *191*, 12–29. https://doi.org/10.1111/j.1365-246X.2012.05609.x

Lavier, L. L., Buck, W. R., & Poliakov, A. N. B. (2000). Factors controlling normal fault offset in an ideal brittle layer. *Journal of Geophysical Research*, *105*(B10), 23431–23442. https://doi.org/10.1029/2000JB900108

Little, T. A., Webber, S., Mizera, M., Boulton, C., Oesterle, J., Ellis, S., et al. (2019). Evolution of a rapidly slipping, active low-angle normal fault, suckling-dayman metamorphic core complex, SE Papua New Guinea. *GSA Bulletin*, *131*(7–8), 1333–1363. https://doi.org/10.1130/b35051.1

MacLeod, C. J., Carlut, J., Escartín, J., Horen, H., & Morris, A. (2011). Quantitative constraint on footwall rotations at the 15°45′N oceanic core complex, mid-Atlantic ridge: Implications for oceanic detachment fault processes. *Geochemistry, Geophysics, Geosystems*, *12*, Q0AG03. https://doi.org/10.1029/2011GC003503

MacLeod, C. J., Escartín, J., Banerji, D., Banks, G. J., Gleeson, M., Irving, D. H. B., et al. (2002). Direct geological evidence for oceanic detachment faulting: The Mid-Atlantic Ridge, 15°45′N. *Geology*, *30*(10), 879–882. https://doi.org/10.1130/0091-7613(2002)030<0879:DGEFOD>2.0.CO;2

MacLeod, C. J., Searle, R., Murton, B., Casey, J., Mallows, C., Unsworth, S., et al. (2009). Life cycle of oceanic core complexes. *Earth and Planetary Science Letters*, *287*(3–4), 333–344. https://doi.org/10.1016/j.epsl.2009.08.016

Mark, H. F., Behn, M. D., Olive, J.-A., & Liu, Y. (2018). Controls on mid-ocean ridge normal fault seismicity across spreading rates from rate-and-state friction models. *Journal of Geophysical Research: Solid Earth*, *123*, 6719–6733

Moresi, L., Dufour, F., & Mühlhaus, H.-B. (2003). A Lagrangian integration point finite element method for large deformation modeling of viscoelastic geomaterials. *Journal of Computational Physics*, *184*(2), 476–497. https://doi.org/10.1016/s0021-9991(02)00031-1

Morris, A., Gee, J., Pressling, N., John, B., MacLeod, C. J., Grimes, C., & Searle, R. (2009). Footwall rotation in an oceanic core complex quantified using reoriented integrated ocean drilling program core samples. *Earth and Planetary Science Letters*, *287*(1–2), 217–228. https://doi.org/10.1016/j.epsl.2009.08.007

Müller, R. D., Seton, M., Zahirovic, S., Williams, S. E., Matthews, K. J., Wright, N. M., et al. (2016). Ocean basin evolution and global-scale plate reorganization events since pangea breakup. *Annual Review of Earth and Planetary Sciences*, *44*, 107–138. https://doi.org/10.1146/annurev-earth-060115-012211

Naliboff, J., Glerum, A., Brune, S., Péron-Pinvidic, G., & Wrona, T. (2020). Development of 3-d rift heterogeneity through fault network evolution. *Geophysical Research Letters*, *47*, e2019GL086611. https://doi.org/10.1029/2019GL086611

Olive, J.-A., & Behn, M. D. (2014). Rapid rotation of normal faults due to flexural stresses: An explanation for the global distribution of normal fault dips. *Journal of Geophysical Research: Solid Earth*, *119*, 3722–3739. https://doi.org/10.1002/2013JB010512

Olive, J.-A., Behn, M. D., Mittelstaedt, E., Ito, G., & Klein, B. Z. (2016). The role of elasticity in simulating long-term tectonic extension. *Geophysical Journal International*, *205*(2), 728–743. https://doi.org/10.1093/gji/ggw044

Parnell-Turner, R., Escartín, J., Olive, J.-A., Smith, D. K., & Petersen, S. (2018). Genesis of corrugated fault surfaces by strain localization recorded at oceanic detachments. *Earth and Planetary Science Letters*, *498*, 116–128. https://doi.org/10.1016/j.epsl.2018.06.034

Parnell-Turner, R., Sohn, R., Peirce, C., Reston, T., MacLeod, C., Searle, R. C., & Simão, N. M. (2020). Seismicity trends and detachment fault structure at 13°N, mid-Atlantic ridge. *Geology*, *49*(3), 320–324.

Parnell-Turner, R., Sohn, R. A., Peirce, C., Reston, T. J., MacLeod, C. J., Searle, R. C., & Simão, N. M. (2017). Oceanic detachment faults generate compression in extension. *Geology*, *45*(10), 923–926. https://doi.org/10.1130/g39232.1

Reston, T., & Ranero, C. R. (2011). The 3-d geometry of detachment faulting at mid-ocean ridges. *Geochemistry, Geophysics, Geosystems*, *12*, Q0AG05. https://doi.org/10.1029/2011GC003666

Rose, I., Buffett, B., & Heister, T. (2017). Stability and accuracy of free surface time integration in viscous flows. *Physics of the Earth and Planetary Interiors*, *262*, 90–100. https://doi.org/10.1016/j.pepi.2016.11.007

Sandiford, D., Moresi, L. M., Sandiford, M., Farrington, R., & Yang, T. (2020). The fingerprints of flexure in slab seismicity. *Tectonics*, *39*, e2019TC005894. https://doi.org/10.1029/2019TC005894

Schouten, H., Smith, D. K., Cann, J. R., & Escartín, J. (2010). Tectonic versus magmatic extension in the presence of core complexes at slow-spreading ridges from a visualization of faulted seafloor topography. *Geology*, *38*(7), 615–618. https://doi.org/10.1130/g30803.1

Spencer, J. E. (1984). Role of tectonic denudation in warping and uplift of low-angle normal faults. *Geology*, *12*(2), 95–98. https://doi.org/10.1130/0091-7613(1984)12<95:ROTDIW>2.0.CO;2

Sullivan, C., & Kaszynski, A. (2019). PyVista: 3d plotting and mesh analysis through a streamlined interface for the visualization toolkit (VTK). *The Journal of Open Source Software*, *4*(37), 1450. https://doi.org/10.21105/joss.01450

Tucholke, B. E. (1998). Discovery of "megamullions" reveals gateways into the ocean crust and upper mantle. *Oceanus-Woods Hole Mass*, *41*, 15–19.

Tucholke, B. E., Behn, M. D., Buck, W. R., & Lin, J. (2008). Role of melt supply in oceanic detachment faulting and formation of megamullions. *Geology*, *36*(6), 455–458. https://doi.org/10.1130/g24639a.1

Tucholke, B. E., Lin, J., & Kleinrock, M. C. (1998). Megamullions and mullion structure defining oceanic metamorphic core complexes on the mid-atlantic ridge. *Journal of Geophysical Research*, *103*(B5), 9857–9866. https://doi.org/10.1029/98JB00167

Wernicke, B., & Axen, G. J. (1988). On the role of isostasy in the evolution of normal fault systems. *Geology*, *16*(9), 848–851. https://doi.org/10.1130/0091-7613(1988)016<0848:OTROII>2.3.CO;2

Yu, Z., Li, J., Niu, X., Rawlinson, N., Ruan, A., Wang, W., et al. (2018). Lithospheric structure and tectonic processes constrained by microearthquake activity at the central ultraslow-spreading southwest Indian ridge (49.2 to 50.8 e). *Journal of Geophysical Research: Solid Earth*, *123*, 6247–6262.